bioRxiv preprint doi: https://doi.org/10.1101/2023.04.24.538108; this version posted April 28, 2023. The copyright holder for this preprint (which was not certified by peer review) is the author/funder, who has granted bioRxiv a license to display the preprint in perpetuity. It is made available under a CC-BY-ND 4.0 International license.

Title: Cell based dATP delivery as a therapy for chronic heart failure.

Authors: Ketaki N Mhatre[1,2,4], Julie Mathieu[1,9], Amy Martinson[1,3,4], Galina Flint[2,5], Leslie P.Blakley[1,3,4], Arash Tabesh[1,4], Hans Reinecke[1,3,4], Xiulan Yang[1,3,4,], Xuan Guan[2], Eesha Murali[1,2], Jordan M Klaiman[1,3,4], Guy L Odom[1,3,5,11], Mary Beth Brown[5,14], Rong Tian[7,5,10], Stephen D Hauschka[1,5,12], Daniel Raftery[7,10,13], Farid Moussavi-Harami[1,3,4,5,8], Michael Regnier[1,2,3,5,6†*], Charles E Murry[1,2,3,4,5,8†*]

Affiliations:
[1]Institute for Stem Cell and Regenerative Medicine, University of Washington; Seattle, WA 98109, USA.
[2]Department of Bioengineering, University of Washington; Seattle, WA 98195, USA.
[3]Center for Cardiovascular Biology, University of Washington; Seattle, WA 98109, USA.
[4]Department of Laboratory Medicine & Pathology, University of Washington; Seattle, WA 98195, USA.
[5]Center for Translational Muscle Research, University of Washington; Seattle, WA 98109, USA.
[6]Department of Physiology and Biophysics, University of Washington; Seattle, WA 98195, USA.
[7]Department of Anesthesiology and Pain Medicine, University of Washington; Seattle, WA 98195, USA.
[8]Division of Cardiology, University of Washington; Seattle, WA 98195, USA.
[9]Department of Comparative Medicine, University of Washington; Seattle, WA 98195, USA.
[10]The Mitochondria and Metabolism Center (MMC), University of Washington; Seattle, WA 98109, USA.
[11]Department of Neurology, University of Washington; Seattle, WA 98195, USA.
[12]Department of Biochemistry, University of Washington; Seattle, WA 98195, USA.
[13]Northwest Metabolomics Research Center, University of Washington; Seattle, WA 98109, USA.
[14]Division of Physical Therapy, Department of Rehabilitation Medicine, University of Washington; Seattle, WA 98195, USA.

[†]These authors contributed equally to this work

*Corresponding author. Email:
Charles E Murry: murry@uw.edu
Michael Regnier: mregnier@uw.edu

Abstract: Transplanted human pluripotent stem cell-derived cardiomyocytes (hPSC-CMs) improve ventricular performance when delivered acutely post-myocardial infarction but are ineffective in chronic myocardial infarction/heart failure. 2'-deoxy-ATP (dATP) activates cardiac myosin and potently increases contractility. Here we engineered hPSC-CMs to overexpress ribonucleotide reductase, the enzyme controlling dATP production. In vivo, dATP-producing CMs formed new myocardium that transferred dATP to host cardiomyocytes via gap junctions, increasing their dATP levels. Strikingly, when transplanted into chronically infarcted hearts, dATP-producing grafts increased left ventricular function, whereas heart failure worsened with wild-type grafts or vehicle injections. dATP-donor cells recipients had greater voluntary exercise, improved cardiac metabolism, reduced pulmonary congestion and pathological cardiac hypertrophy, and improved survival. This combination of remuscularization plus enhanced host contractility offers a novel approach to treating the chronically failing heart.

WITHDRAWN
see manuscript BCH for details

bioRxiv preprint doi: https://doi.org/10.1101/2023.04.24.538108; this version posted April 28, 2023. The copyright holder for this preprint (which was not certified by peer review) is the author/funder, who has granted bioRxiv a license to display the preprint in perpetuity. It is made available under a CC-BY-ND 4.0 International license.

One Sentence Summary: Transplanting gene-edited dATP-donor cardiomyocytes in chronically infarcted heart restores their cardiac function, improving both exercise tolerance and survival.

Main Text:

Ischemic heart disease is the number one cause of death worldwide (*1*). In myocardial infarction (MI), commonly known as a 'heart attack', the obstruction of a coronary artery results in cardiomyocyte (CM) cell death. Since the adult myocardium has no regenerative capacity, recovery is limited and proceeds by scar formation, interstitial fibrosis, and CM hypertrophy, with a maladaptive myocardium remodeling that leads to wall thinning, ventricular dilation, and progressive heart failure (HF) (*2*). Pharmacological treatments for chronic ischemic HF, such as neurohumoral blockade or diuretics, alleviate downstream sequelae but do not address the root causes of CM deficiency and impaired contractility of surviving CMs (*3*). No curative remedies are available, leaving heart transplantation as the only option for patients with severe chronic HF (*4*).

In recent years, regenerative therapies have focused on developing human pluripotent stem cell-derived cardiomyocytes (hPSC-CMs) for the treatment of HF resulting from MI, leading to early clinical trials (*5–8*). Previously, we and other groups have demonstrated that hPSC-CMs can remuscularize experimental infarcts, integrating and beating in synchrony with the host myocardium (*9*, *10*). In subacute models of MI, these cells directly contribute to contractile function (*11*) and attenuate adverse ventricular remodeling and progressive heart failure (*12*). Enigmatically, despite clear benefits after acute injury, hPSC-CMs have not been effective in improving the lost contractile function in chronic MI (*13*, *14*), perhaps because of widespread host cardiomyocyte dysfunction in chronic heart failure. Thus, hPSC-CMs require an upgrade to reach their full potential to be cardio-regenerative and restorative as an effective treatment for established HF.

WITHDRAWN
see manuscript for details

We previously demonstrated that dATP, a naturally occurring nucleotide produced by ribonucleotide reductase (RNR), is a potent allosteric myosin activator with multiple cardiac benefits (*15*). In viral gene therapy and transgenic mice models, we have overexpressed RNR to elevate cellular dATP levels that resulted in 1) stronger, faster contraction and relaxation of cardiomyocytes *in vitro* (*16*, *17*), 2) rescue of left ventricular (LV) function in acutely infarcted rat and pig hearts via gene therapy (although viral transduction in the pig was not sufficiently robust to support clinical development) (*17*, *18*), and 3) improvement of cardiac aerobic metabolism in a transgenic mouse model (*19*). Importantly, we have shown that dATP can spread through the myocardium via gap junctions, thereby increasing contractility in a non-cell autonomous manner (*20*). Together, these studies highlight multiple effects of dATP elevation that contribute to enhanced cardiac function. Hence, we hypothesized that engineering hPSC-CMs to act as factory cells that produce and deliver dATP to the native myocardium would improve cardiac function when delivered during chronic MI.

Results

Generation of genome-edited hPSC-CMs to elevate the cardiac inotrope, dATP.

Our overall strategy was to engineer the hPSC-CMs to produce a sufficient elevation of dATP so that they engraft and diffuse dATP to the chronic MI heart (Fig. 1A).

RNR is the key enzyme that regulates the synthesis of deoxynucleotide triphosphates, including dATP. The enzyme is a hetero tetramer consisting of a large subunit, R1, and one of two small isoform subunits, R2 or R2b, encoded by RRM1 and RRM2 or RRM2B, respectively. The large R1 subunit contains a catalytic site, and the small subunit (R2 or R2b) contains the free radical generator that,

bioRxiv preprint doi: https://doi.org/10.1101/2023.04.24.538108; this version posted April 28, 2023. The copyright holder for this preprint (which was not certified by peer review) is the author/funder, who has granted bioRxiv a license to display the preprint in perpetuity. It is made available under a CC-BY-ND 4.0 International license.

together with the catalytic site, removes oxygen from the 2' position of the ribose ring. RRM2 is tightly regulated by the ubiquitin-proteasome pathway to maintain its activity during the cell cycle but is down-regulated in non-dividing cell states (*21*). This proteasomal degradation poses a challenge to its stable expression in post-mitotic CMs.

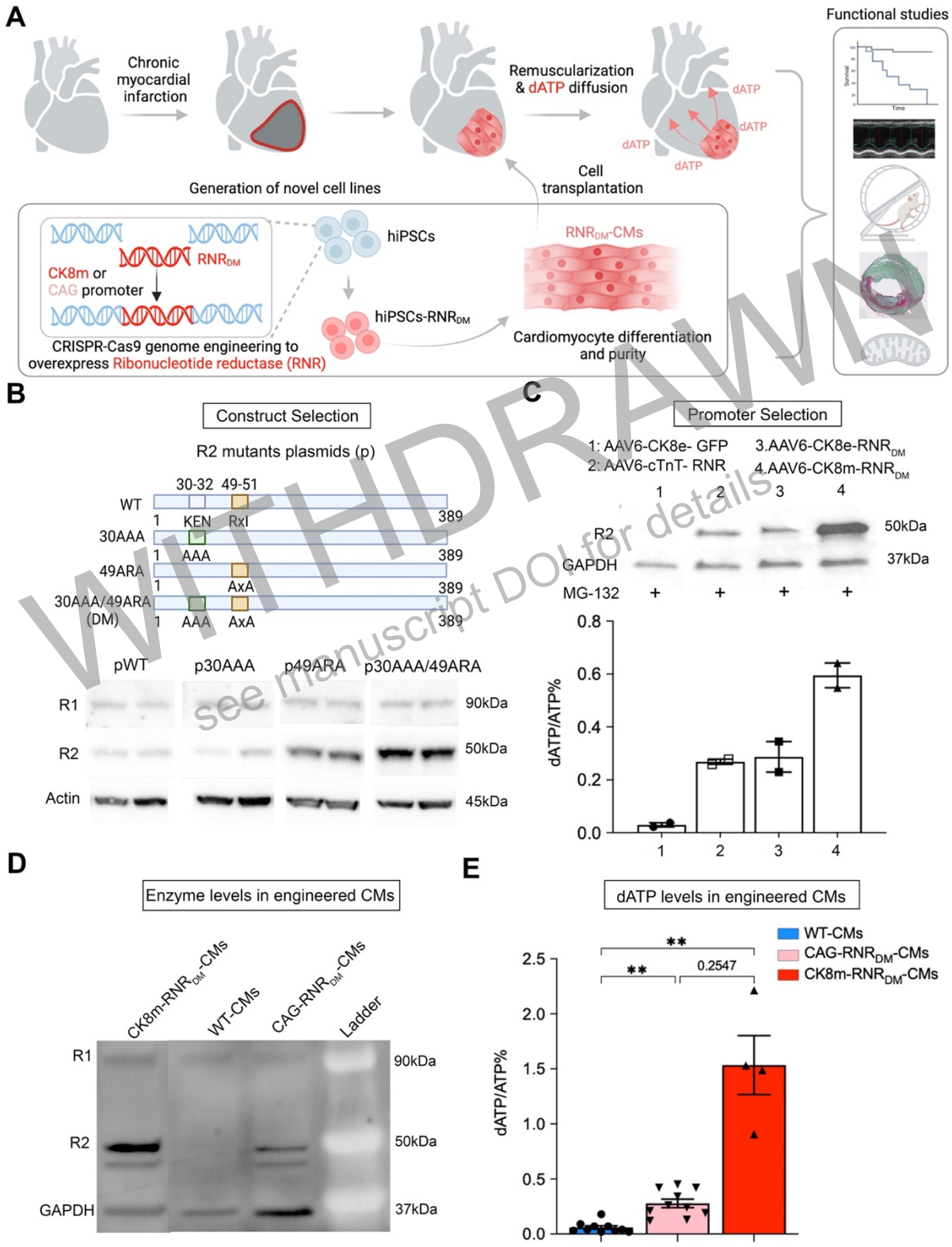
To alleviate this problem, we designed a double mutant R2 (RNR_{DM}) with mutations at the two critical recognition sites for ubiquitination and proteolysis (the KEN box at amino acid residues 30-32 and cyclin-binding domain 49RxL) to stabilize R2 (*22*, *23*). Using site-directed mutagenesis in RRM2, we converted the KEN box to AAA and the 49RxL to AxA, both individually and in combination. Transfection of WT-CMs with equal amounts of plasmids containing different R2 mutants showed that double R2 mutants gave the highest enzyme levels (Fig. 1B). Thus, we chose the RNR_{DM} construct with both mutations for maximum R2 stability in hPSC-CMs.

To express high levels of RNR in hPSC-CMs, we initially tested the strong and constitutively expressed CAG promoter, then subsequently tested three strong muscle-specific promoters (cTnT, CK8e, and CK8m; the CK8e and CK8m promoters are derived from the muscle creatine kinase promoter). hPSC-CMs were transduced with equal amounts of different adeno-associated viral vectors, serotype-6 (AAV6), carrying each of the three promoters driving RNR or RNR_{DM} expression. The proteosome inhibitor MG-132 was added to inhibit proteolysis of RNR. R2 expression and dATP/ATP percentage were highest in cells that received AAV6-CK8m-RNR_{DM} (Fig 1C). Hence, we chose the CK8m promoter to express RNR_{DM} for the second dATP-donor hPSC cell line.

Next, we used CRISPR-Cas9 technology to knock either the CAG-RNR_{DM} or the CK8m-RNR_{DM} cassette into the AAVS1 safe harbor locus of WTC11 hiPSCs (Figs S1, S2, and S3). Two hiPSC lines (CAG-RNR_{DM} (clone #7)) and CK8m-RNR_{DM} (clone #15)) were selected that exhibited the highest R1 and R2 protein levels as differentiated CMs (Fig 1D and Fig S2B, C). ATP and dATP assays via HPLC-MS/MS (*24*) showed that the CAG-RNR_{DM}- and CK8m-RNR_{DM}-CMs had 4.7- and 26-fold elevation of dATP levels (dATP/ATP%: 0.28±0.03% and 1.5±0.3%, respectively), compared with WT-CMs (0.059±0.01%) (Fig. 1e). Elevated dATP levels were consistent across multiple sets of differentiated CAG-RNR_{DM} and CK8m-RNR_{DM} cell lines, thus confirming stable RNR enzyme activities.

WITHDRAWN
See manuscript for details

bioRxiv preprint doi: https://doi.org/10.1101/2023.04.24.538108; this version posted April 28, 2023. The copyright holder for this preprint (which was not certified by peer review) is the author/funder, who has granted bioRxiv a license to display the preprint in perpetuity. It is made available under a CC-BY-ND 4.0 International license.



WITHDRAWN see manuscript DOI for details

Fig. 1. Generation of stable genome edited hiPSC cell lines and resultant dATP elevation. (A) Strategy to improve cell therapy for chronic myocardial infarction **(B)** Schematic representation of WT R2 highlighting recognition sites for ubiquitination and proteolysis and the more stable R2 mutants produced by site directed mutagenesis. Representative immunoblot (below) showing R1 and R2 levels in the hPSC-CMs transfected with expression plasmid containing different R2 mutants (N=2) **(C)** Promoters cTnT, CK8e and CK8m were screened for R2 expression (immunoblot) and ratio of dATP

bioRxiv preprint doi: https://doi.org/10.1101/2023.04.24.538108; this version posted April 28, 2023. The copyright holder for this preprint (which was not certified by peer review) is the author/funder, who has granted bioRxiv a license to display the preprint in perpetuity. It is made available under a CC-BY-ND 4.0 International license.

to ATP % levels (bar graph) in the hPSC-CMs transduced with AAV6 vectors carrying different promoters driving R2 expression (N=1) along with proteasome and calpain inhibitor MG-132. Each symbol represents technical replicate (solid circle (CK8e-GFP), open square (cTnT-RNR), solid squares (CK8e-RNR_{DM}), and solid triangles (CK8m-RNR_{DM}). **(D)** Representative immunoblot showing expression of R2 subunit in cardiomyocytes derived from selected CAG and CK8m-RNR_{DM} clone's vs WT cells (lanes are rearranged for presentation purposes). **(E)** Bar graph showing the ratio of dATP to ATP % in WT-CMs, CAG and CK8m-RNR_{DM}-CMs. Each symbol represents biological replicate (solid circle (WT), solid inverted triangles (CAG-RNR_{DM}-CMs), solid triangles (CK8m-RNR_{DM}-CMs)). N>3 directed differentiation. All data are presented as mean ± S.E.M. P values were determined using Kruskal-Wallis test with Dunn's correction for multiple comparisons (**p<0.01). (Panels A and B were created with Biorender.com)**.**

Enhanced cardiac function positively correlates with increased dATP levels.

We next assessed whether the transplantation of CAG-RNR_{DM}- and CK8m-RNR_{DM}-CMs results in engraftment and elevation of dATP in the host myocardium, subsequently increasing cardiac function. Naïve athymic rats were injected intramyocardially with either CAG-RNR_{DM}-CMs, CK8m-RNR_{DM}-CMs, or WT-CMs ($10x10^6$ cells) in a pro-survival cocktail (PSC). These were compared with a no-cells (PSC-only) control (Fig 2a). The CAG-RNR_{DM}- and CK8m-RNR_{DM}-CMs preparations employed for this study had a cardiac purity and R2 co-expression of >80%, as determined by flow cytometry (fig S3B).

Prior to cell transplantation, baseline echocardiography showed that all groups exhibited similar fractional shortening (%FS) (41.8±0.6%). At 4-weeks following transplantation, animals receiving WT-CMs, or vehicle had a similar %FS (38.6±1.4% and 41.04±2.4%, respectively). In contrast, %FS was improved in CAG-RNR_{DM}- and CK8m-RNR_{DM}-CMs recipients from their baseline values (45.8 ± 0.8% and 47.7±0.6%, p<0.01) (Fig. 2B, C, table S1). This was significantly greater than WT-CMs recipients at 4 weeks post-transplantation (p<0.01, Fig. 2B). The elevation of %FS by CAG-RNR_{DM}-CMs required 4 weeks to achieve statistical significance, whereas the CK8m-RNR_{DM}-CMs hearts had increased %FS by 1-week and a maximal increase by 2-weeks post-transplant (Fig. 2B, C). Animals receiving CAG-RNR_{DM}- and CK8m-RNR_{DM}-CMs had comparable heart weights (table S1), heart rates (table S1), and LV end-diastolic dimensions (LVEDD) at both 2- and 4-weeks post-transplantation compared to WT-CMs recipients (table S1). This suggests the increase in FS% was due to the inotropic effect of elevated cardiac dATP independent of ventricular remodeling (Fig. 2D). Overall, both the CAG-RNR_{DM}- and CK8m-RNR_{DM}-CMs increased contractility of the uninjured heart, with the higher dATP-producing CK8m-RNR_{DM}-CMs yielding faster increases.

To investigate the dynamics of dATP diffusion from cell grafts to host myocardium at 4-weeks post-transplant, we measured dATP levels in different zones of the heart using HPLC-MS/MS (Fig. 2D). The cardiac apex (site of cell transplantation, fig. S4) had the highest levels of dATP in animals receiving CK8m-RNR_{DM}-CMs, with progressively lower levels in the border zone and the remote myocardium (Fig. 2D). In the apex, dATP levels were significantly elevated in CAG-RNR_{DM}- and CK8m-RNR_{DM}-CMs recipients as compared to vs. WT-CMs (0.11% of ATP levels (p<0.05) vs. 0.41±0.17% (p<0.01) vs. 0.03±0.01%, respectively. There was also a trend toward higher dATP levels in the border zone and remote myocardium in hearts receiving the CAG-RNR_{DM}- or CK8m-RNR_{DM}-CMs, though values were not statistically different due to fewer animals tested. We found a strong positive correlation between dATP levels in the apex and cardiac function at 4-weeks post-transplant for both the CAG-RNR_{DM}- and CK8m-RNR_{DM}-CMs recipient's hearts (CAG-RNR_{DM}-CMs, R^2=0.96, p=0.1, N=3; CK8m-RNR_{DM}-CMs, R^2=0.76, p=0.1, N=4; Fig. 2E). Histology of these hearts showed successful integration of CAG-RNR_{DM}- and CK8m-RNR_{DM}-CMs grafts with formation of adherens

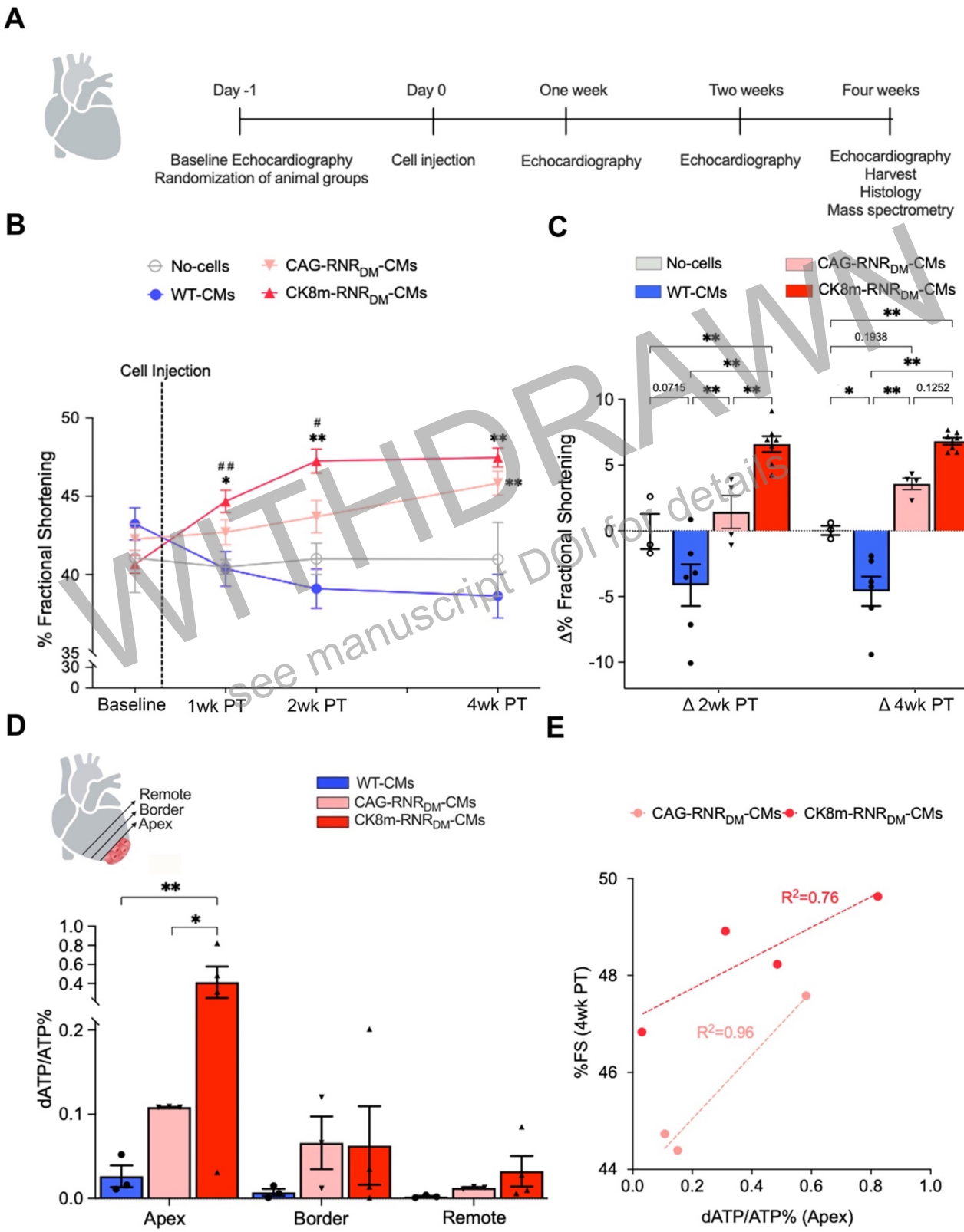
WITHDRAWN
See manuscript DOI for details

bioRxiv preprint doi: https://doi.org/10.1101/2023.04.24.538108; this version posted April 28, 2023. The copyright holder for this preprint (which was not certified by peer review) is the author/funder, who has granted bioRxiv a license to display the preprint in perpetuity. It is made available under a CC-BY-ND 4.0 International license.

and gap junctions between graft and host (fig. S4, S5), consistent with our previous reports for WT-CMs engraftment (*25*).

WITHDRAWN
see manuscript DOI for details

bioRxiv preprint doi: https://doi.org/10.1101/2023.04.24.538108; this version posted April 28, 2023. The copyright holder for this preprint (which was not certified by peer review) is the author/funder, who has granted bioRxiv a license to display the preprint in perpetuity. It is made available under a CC-BY-ND 4.0 International license.



WITHDRAWN
see manuscript DOI for details

Fig. 2. dATP- producing cardiomyocyte grafts increase contractility in healthy hearts. (A) Study timeline **(B)** Echocardiographic evaluation at baseline, 1 – 4 weeks (wk) post-transplantation (PT) **(C)** Δ% Fractional shortening, difference between baseline and 2-, 4- wk PT, N= No-cells (3), WT (6), CAG -RNR$_{DM}$-CMs (4), CK8m-RNR$_{DM}$-CMs (7). **(D)** dATP to ATP % measured by mass spectrometry at apex (cell injection sites), border and remote zones at the 4-wk PT endpoint, N= WT 7

bioRxiv preprint doi: https://doi.org/10.1101/2023.04.24.538108; this version posted April 28, 2023. The copyright holder for this preprint (which was not certified by peer review) is the author/funder, who has granted bioRxiv a license to display the preprint in perpetuity. It is made available under a CC-BY-ND 4.0 International license.

(3), CAG-RNR$_{DM}$-CMs (3), CK8m-RNR$_{DM}$-CMs (4). **(E)** Scatter plot of %FS at 4-wk PT plotted as a function of dATP to ATP % measured 4-wk PT in apex. Each symbol represents biological replicate (solid circle (WT), Solid inverted triangles (CAG-RNR$_{DM}$-CMs), Solid triangles (CK8m-RNR$_{DM}$-CMs). All data are presented as mean ± S.E.M. P values for %FS vs. timepoint, Δ%FS vs. timepoint, and dATP/ATP% vs zones were determined using repeated measure 2-way ANOVA with Tukey's multiple comparison test, *P<0.05, **P<0.01 vs. WT-CMs; #P<0.05, ##P<0.01 vs. No-cells. (Panel A and D were created with Biorender.com).

Transplanted CK8m-RNR$_{DM}$-CMs improve cardiac function, exercise capacity, and survival in chronic myocardial infarction.

To test the hypothesis that CK8m-RNRDM-CMs would improve cardiac function in a chronic MI model (Fig. 3A), the cells were transplanted 1-month after ischemia-reperfusion (I/R) injury. We chose to use CK8m-RNR$_{DM}$-CMs due to their superior improvements in LV function in non-infarcted hearts. Prior to infarction, all groups exhibited normal cardiac function (%FS 44.6±0.3%; Fig. 3C). At 1-month post-injury, when chronic MI was established, animals were enrolled into 3 groups (N= No-cells (10), WT-CMs (14), CK8m-RNR$_{DM}$-CMs (16)), designed to have comparable pre-transplantation %FS. Accordingly, 1-month post I/R, cardiac function decreased to a similar extent in all animal groups (average %FS; No-cells: 29.5%±2.5%, WT: 29.2±1.7%, CK8m-RNR$_{DM}$-CMs: 25.2±1.3%) (Fig. 3C; table S2). The cell transplantation at 1-month post-I/R and echocardiography scans and interpretations at baseline (1-month post-I/R) and 1-, 2-, and 3-months post-transplantation were done in a blinded manner. Ten million CMs of each genotype or vehicle control were injected into the central ischemic and lateral border zones of the scar. Prior experience led us to expect significant mortality associated with the chronic MI model (*14*, *25*). Indeed, 40% of the No-cells control group died by the end of the 3-month post-transplantation period. Interestingly, only 1 of the 14 animals from the WT-CMs group died (7.1%), and none of the 16 animals receiving CK8m-RNR$_{DM}$-CMs died. Kaplan–Meier curves showed that the difference in percent survival within the three animal groups is significant (Fig. 3B) (P<0.01).

WITHDRAWN see manuscript DOI for details

From 1- to 3-months post-transplantation, the No-cells recipients continued to have significant reductions in cardiac function (%FS average: 24.3±2.6, 20.6±1.1 and 18.5±1.1; respectively). Confirming our previous observations (*14*), recipients of WT cells showed no %FS benefit when transplanted at one month post-I/R, and their functional trajectory from 1–to 3-months post-transplantation overlapped with the No-cells group (Fig. 3C, D; fig. S6A). In stark contrast, animals receiving CK8m-RNR$_{DM}$-CMs began to recover function by 1-month post-transplant (Fig. 3C, D; fig. S6A) and at 2- and 3- months exhibited significantly higher %FS than WT-CMs and No-cells groups (P<0.01). Cardiac function recovery continued to improve at the 3-month post-transplantation endpoint (Fig. 3D), where %FS in CK8m-RNR$_{DM}$-CMs recipients averaged 29.7±1.1% vs. 19.5±1.8% in WT-CM and 18.5±1.1% in No-cells controls (P<0.01 CK8m-RNR$_{DM}$-CMs vs. WT-CMs or No-cells group; Fig. 3C, D; fig. S6A; table S2).

We also explored the progression of heart failure by examining each animal's Δ%FS from baseline (Fig. 3D). The No-cells and WT-CMs recipients showed similar decreases over the 3-month post-transplantation observation, reaching -10.4±2.6% in No-cells recipients and -10.3±1.9% in WT-CM recipients. Strikingly, CK8m-RNR$_{DM}$-CMs recipients showed significant increases in Δ%FS at 1-, 2-, and 3-months post-transplant, averaging +1.9±0.8%, +2.7±0.9%, and +4.5±1.0% relative to the baseline function (P≤0.01 compared to WT and No-cells recipients; Fig. 3D). Left ventricular end-systolic dimension (LVESD) increased from 1-3-months post-transplantation in both No-cells and WT-CMs recipients, indicating significant systolic dysfunction. In contrast, there was a significant

bioRxiv preprint doi: https://doi.org/10.1101/2023.04.24.538108; this version posted April 28, 2023. The copyright holder for this preprint (which was not certified by peer review) is the author/funder, who has granted bioRxiv a license to display the preprint in perpetuity. It is made available under a CC-BY-ND 4.0 International license.

reduction in LVESD in the CK8m-RNR$_{DM}$-CMs recipients (fig. S6B). For left ventricular end-diastolic dimension (LVEDD), the data trended towards lower LVEDD in CK8m-RNR$_{DM}$-CMs recipients ($p=0.06$ vs. No-cells, $p=0.13$ vs. WT) (fig. S6C). Together, these data demonstrate that dATP-donor hiPSC-CM reverse the progression of heart failure in chronically infarcted rats, principally through benefitting systolic function with a minor trend toward reduced LV remodeling.

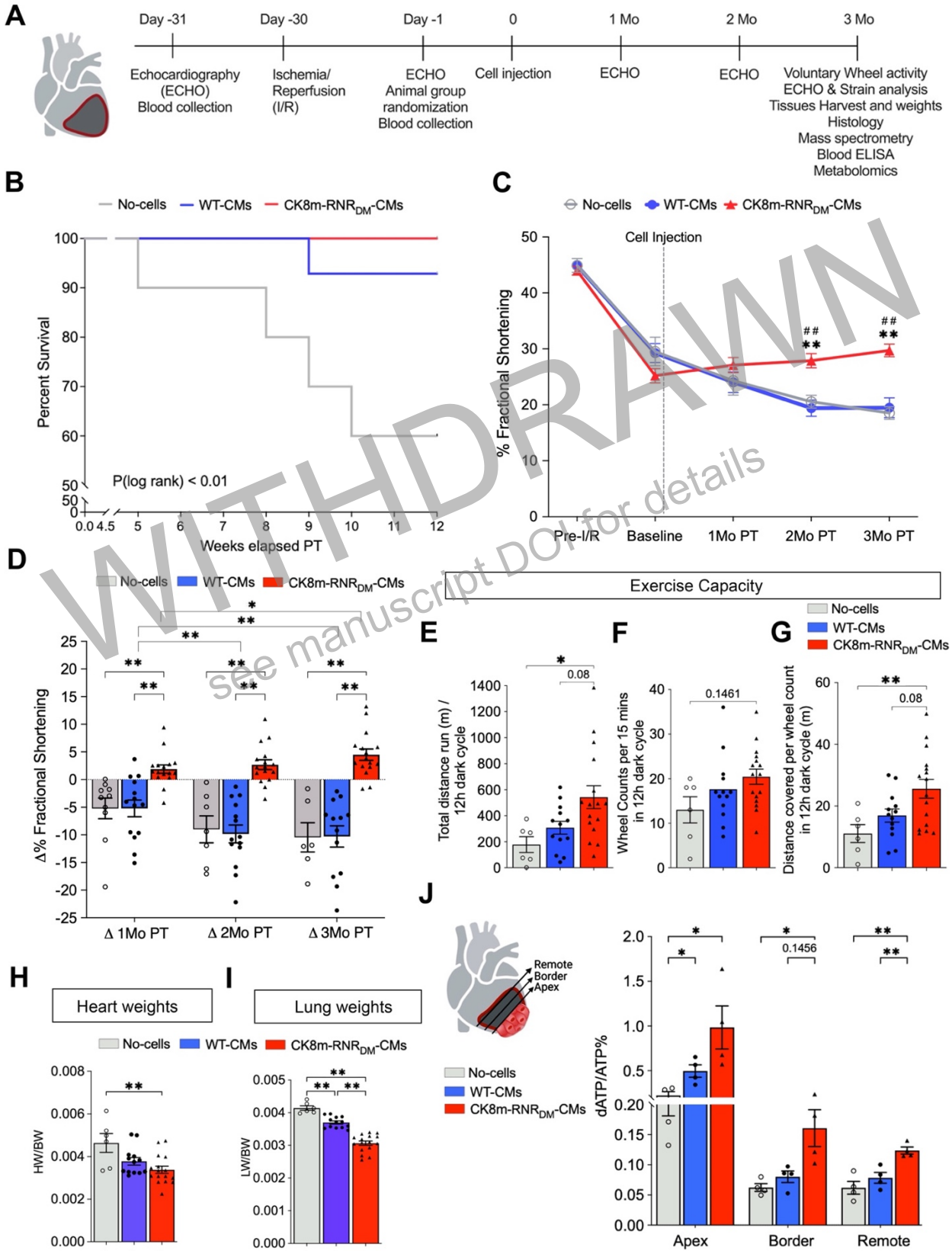
Along with depressed cardiac function, chronic HF patients exhibit exercise intolerance, fatigue, and exertional dyspnea (*26*). Hence, we evaluated exercise tolerance by assessing voluntary wheel running over a single 12-hour period (second dark cycle) (*27*, *28*). There was no significant difference between the No-cells and WT-CMs in wheel activity (Fig. 3E, F G; fig. S6D). However, the recipients of CK8m-RNR$_{DM}$-CMs recipients ran 3.04±1.4-fold further than the No-cells group ($p<0.05$) and trended ($p=0.08$) for further running distance compared to the WT-CMs group (Fig. 3E). The enhanced exercise occurred principally through greater distance run per wheel engagement, with a non-significant trend toward increased wheel engagements (Fig. 3F, 3G, S6D).

In addition to measuring changes in cardiac function, we also measured heart weight, lung weight, and plasma BNP levels as markers of chronic HF. The CK8m-RNR$_{DM}$-CMs recipients had the lowest heart weights (HW/BW) of any group, indicating a significant sparing of cardiac hypertrophy compared to the No-cells group (Fig. 3H). Similarly, the CK8m-RNR$_{DM}$-CMs group had the lowest lung weights (LW/BW) ($p<0.01$) and plasma BNP levels (fig. S7A, B) of any group, indicating reduced pulmonary congestion/edema and reduced cardiac congestion ($p<0.01$; Fig. 3I). The WT group also had significantly lower LW/BW compared to the No-cells controls ($p<0.01$; Fig. 3I). Interestingly, voluntary exercise activity showed a high correlation with LW/BW, %FS, and HW/BW ($R^2 > 0.7$, >0.5, >0.3 respectively in each group; fig. S7C-E).

To test whether these functional improvements correlated with the diffusion of dATP from the donor cells, we measured dATP levels in different zones of the heart at 3-month post-transplantation. Using mass spectrometry, we confirmed that the highest levels of dATP were in the apical heart sections (injection site) of animals. Animals injected with CK8m-RNR$_{DM}$-CMs had the greatest dATP/ATP contents (Fig. 3J; CK8m-RNR$_{DM}$-CMs = 0.98±0.24% vs WT-CMs = 0.5±0.07% vs No-cells = 0.22±0.04%). Most importantly, significantly higher dATP/ATP% was also found in the border (2.7-fold and $p\leq0.05$ vs. No-cells) as well as remote myocardium (2-Fold and $p\leq0.01$ vs. No-cells, 1.6-Fold, and $p\leq0.01$ vs. WT-CMs) in CK8m-RNR$_{DM}$-CMs recipients (Fig. 3J).

WITHDRAWN
see manuscript DOI for details

bioRxiv preprint doi: https://doi.org/10.1101/2023.04.24.538108; this version posted April 28, 2023. The copyright holder for this preprint (which was not certified by peer review) is the author/funder, who has granted bioRxiv a license to display the preprint in perpetuity. It is made available under a CC-BY-ND 4.0 International license.



WITHDRAWN
see manuscript DOI for details

Fig. 3 CK8m-RNR$_{DM}$-CMs transplantation improve cardiac function in chronic myocardial infarction (A) Study design of cell injection in chronic MI model **(B)** Percent survival (P = 0.0076 using one-sided log-rank test) post transplantation (PT) between the groups. **(C)** Mean % Fractional shortening at Pre-I/R, Baseline (BL) 1-month post MI, and 1-3-months (Mo) PT **(D)** Δ% Fractional

bioRxiv preprint doi: https://doi.org/10.1101/2023.04.24.538108; this version posted April 28, 2023. The copyright holder for this preprint (which was not certified by peer review) is the author/funder, who has granted bioRxiv a license to display the preprint in perpetuity. It is made available under a CC-BY-ND 4.0 International license.

shortening, difference between %FS at BL and the timepoints. N=No-cells (10), WT-CMs (14), CK8m-RNR$_{DM}$-CMs (16). **(E)** Total distance run in the second 12h dark cycle. **(F)** Wheel counts per 15mins in the second 12h dark cycle. **(G)** Distance covered per wheel count in the second 12h dark cycle. N= No-cells (6), WT-CMs (13), CK8m-RNR$_{DM}$-CMs (16). **(H)** Heart weight/Body weight (HW/BW) **(I)** Lung weight/Body weight (LW/BW) at the 3 months post transplantation. N= No-cells (10), WT (13), CK8m-RNR$_{DM}$-CMs (16). **(J)** dATP to ATP % at apex, border, and remote zones at the 3-Mo PT. N= No-cells (4), WT-CMs (4), CK8m-RNR$_{DM}$-CMs (4). Each symbol represents biological replicate (open circles (No-cells), solid circle (WT-CMs), Solid triangles (CK8m-RNR$_{DM}$-CMs)). All data are presented as mean ± S.E.M. P values for %FS vs. timepoint, Δ %FS vs. timepoint, dATP/ATP% vs. zones were determined using repeated measure 2-way ANOVA with Tukey's multiple comparison test. P value for exercise capacity measurements were determined using 1-way ANOVA with Dunnett's correction and with Sidak's correction (LW/BW). P values for HW/BW were determined using Kruskal-Wallis with Dunn's correction. *P≤0.05, **P≤0.01. (Panel A and J were created with Biorender.com).

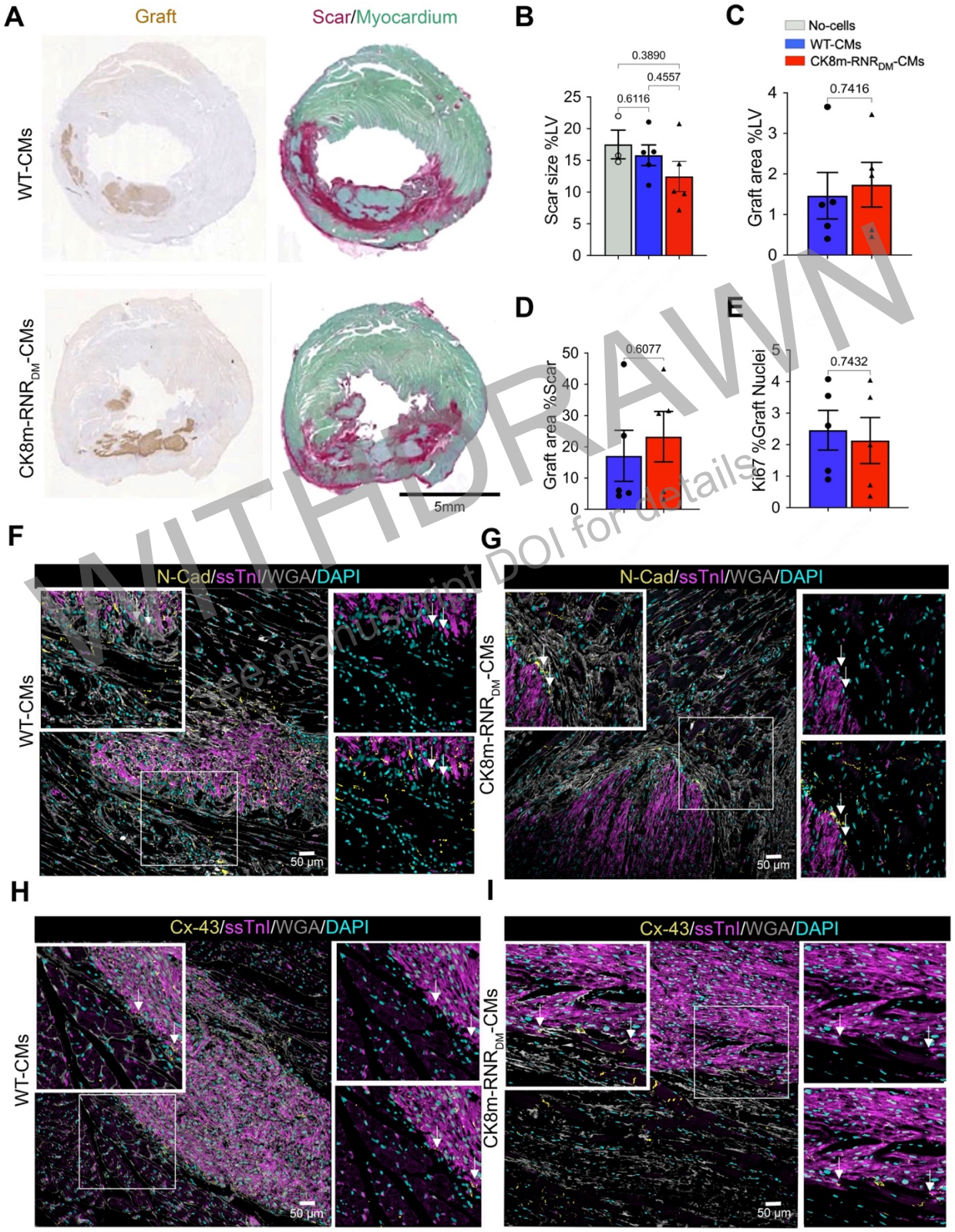
CK8m-RNR$_{DM}$-CMs form comparable grafts to WT cells in chronic myocardial infarction.

Histological analysis was used to compare infarct size, graft size and integration, and the consequences of long-term expression of RNR$_{DM}$ on graft properties. Morphometric measurements at 3-months post-transplantation showed that all groups had nearly transmural scars with a thin rim of spared subepicardial myocardium. Scar sizes were similar in all the groups (Fig. 4A, B), indicating consistency in performing I/R surgical procedures and no effect of the treatment on the scar at 3-months post-transplantation. Immunostaining against human slow skeletal Troponin I (ssTnI, a developmental isoform not expressed in the host adult rat myocardium) (Fig. 4A) showed comparable graft sizes occupying 1.5±0.6% and 1.7±0.5% of the total LV area in WT-CMs and CK8m-RNR$_{DM}$-CMs recipients, respectively (Fig. 4C). Furthermore, the % area occupied by graft compared with total scar area was similar for the recipients of WT and CK8m-RNR$_{DM}$-CMs, respectively (17.1±8.1% and 23.2±8.0%) (Fig. 4D), suggesting similar remuscularization and fibrosis between the groups. Double immunolabelling for ssTnI and Ki67 (a marker for cell proliferation) showed no differences in the percentage of Ki67+ cells in either group (Fig. 4E; fig. S8A, B), suggesting no effect of RNR overexpression on cell proliferation in the grafts. Thus, the quantity and proliferation rates between transplanted WT-CMs and CK8m-RNR$_{DM}$-CMs were similar.

In addition to expressing ssTnI, both WT and CK8m-RNR$_{DM}$ grafts co-expressed the more mature cardiac TnI (cTnI) isoform (fig. S9A, B) and had almost entirely switched from the expression of myosin light chain 2a to myosin light chain 2v (fig. S9C, D). This indicates that the grafts are maturing at comparable rates. Immunolabelling analysis showed that CK8m-RNR$_{DM}$-CMs grafts expressed the cell adhesion molecule, N-cadherin (Fig. 4F, G), between the host and graft interface and formed effective gap junctions (connexin43+) essential for dATP diffusion (*20*) between the graft and the host (Fig. 4H, I). Finally, both WT and CK8m-RNR$_{DM}$ grafts contained vessels that immunolabeled with the endothelial marker, CD31 (fig. S8C, D). In summary, histology shows that CK8m-RNR$_{DM}$-CMs integrated effectively within chronic scar tissue and formed stable, maturing, and vascularized cardiac grafts.

WITHDRAWN
see manuscript DOI for details

bioRxiv preprint doi: https://doi.org/10.1101/2023.04.24.538108; this version posted April 28, 2023. The copyright holder for this preprint (which was not certified by peer review) is the author/funder, who has granted bioRxiv a license to display the preprint in perpetuity. It is made available under a CC-BY-ND 4.0 International license.



WITHDRAWN
See manuscript DOI for details

Fig. 4 Remuscularization of mature scar by CK8m-RNR$_{DM}$-CMs (A) Low-magnification photomicrographs of representative hearts from both groups at 3-months after transplantation. Graft myocardium expressed ssTnI and scar by Picrosirius red. Bar graph depicting **(B)** Scar size %LV **(C)** Graft area % LV **(D)** Scar area % LV per group **(E)** quantification of graft cell expressing proliferation marker Ki67 at 3 months post transplantation. N= No-cells (3), WT (5), CK8m-RNR$_{DM}$-CMs (5). Each

bioRxiv preprint doi: https://doi.org/10.1101/2023.04.24.538108; this version posted April 28, 2023. The copyright holder for this preprint (which was not certified by peer review) is the author/funder, who has granted bioRxiv a license to display the preprint in perpetuity. It is made available under a CC-BY-ND 4.0 International license.

symbol represents biological replicate (open circle (No-cells), solid circle (WT), Solid triangles (CK8m-RNR$_{DM}$-CMs)). Representative image of immunofluorescence staining of the N-Cadherin (N-Cad) (white arrows) between graft and host in **(F)** WT-CMs and **(G)** CK8m-RNR$_{DM}$-CMs recipient. Representative image of immunofluorescence staining of the Connexin 43 (Cx-43) (white arrows) between graft and host in **(H)** WT-CMs and **(I)** CK8m-RNR$_{DM}$-CMs recipient. All data are presented as mean ± S.E.M. P value were determined using Student t-test.

CK8m-RNR$_{DM}$-CMs shift failing heart metabolism towards aerobic respiration.

Chronically failing hearts face a severe energy deficit to support continual cardiac function (*29*). Hence it is important to know if the increased work resulting from CK8m-RNR$_{DM}$-CMs contributes to the failing heart's energy deficit or if it allows for metabolic remodeling toward a more energetically efficient myocardium.

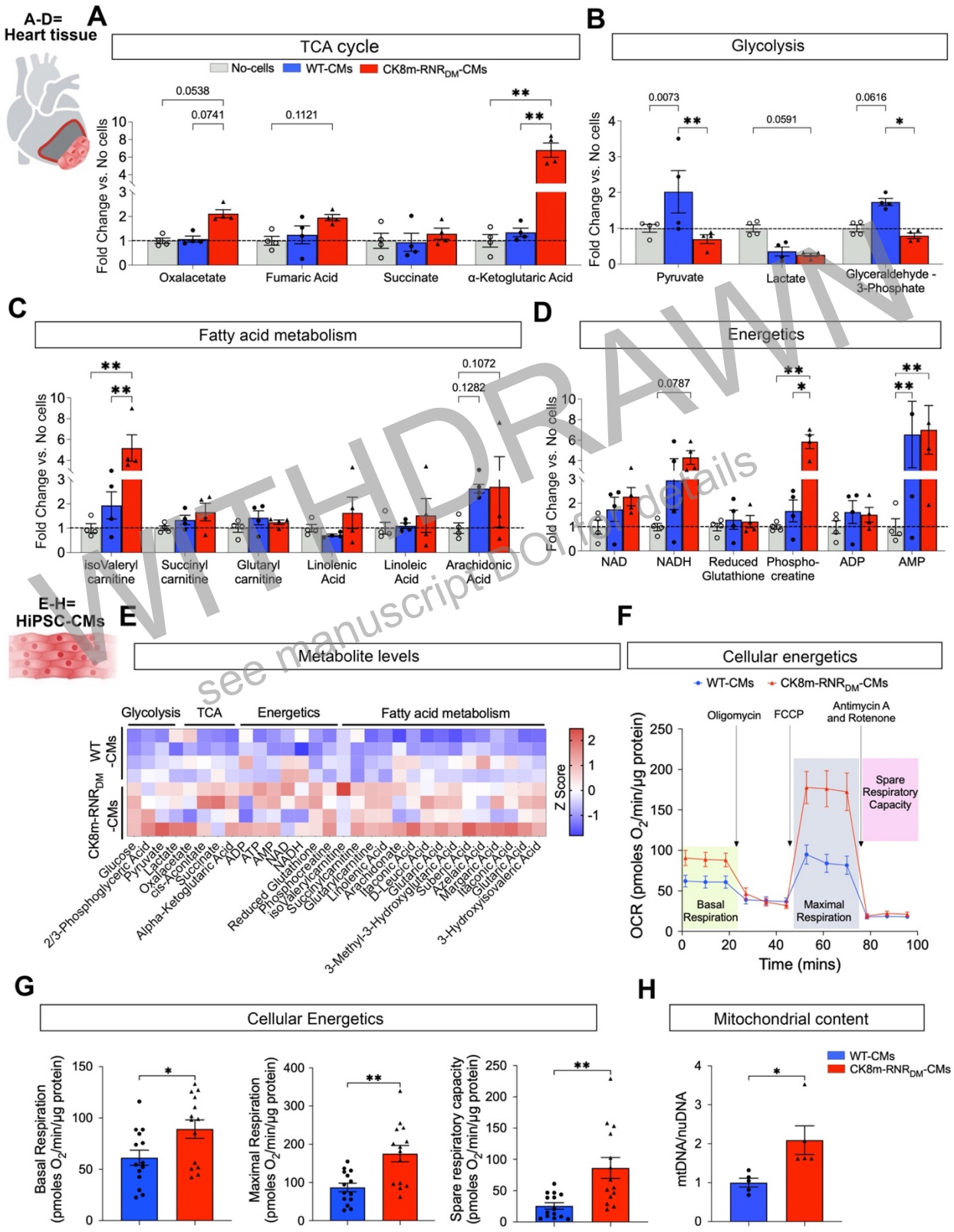
To address this question, we performed targeted metabolomic profiling on LV tissue at 3-months post transplantation by liquid chromatography–mass spectrometry (LC-MS/MS). Substantial differences were identified for CK8m-RNR$_{DM}$-CMs recipient hearts compared to other groups (fig. S10A, B). There were greater levels in most of the tricarboxylic acid cycle (TCA) intermediates (Fig. 5A) and lower levels of glycolytic intermediates (Fig. 5B) in CK8m-RNR$_{DM}$-CMs recipient hearts. In the fatty acid metabolism pathway, acyl-carnitines and (poly)-unsaturated metabolites such as linolenic acid, linoleic acid, and arachidonic acid (Fig. 5C) were also greater in CK8m-RNR$_{DM}$-CMs hearts, suggesting a higher fatty acid supply and oxidation. These data indicates that CK8m-RNR$_{DM}$-CMs recipients' hearts have an oxidative profile, while both WT-CMs and No-cells recipients were more dependent on glycolytic metabolism. We also found higher levels of energetic metabolites (NAD^+, NADH, AMP, and phosphocreatine (pCr)) in the hearts of CK8m-RNR$_{DM}$-CMs recipients as compared to the No-cells and WT group (Fig. 5D).

We next sought to investigate the mechanisms underlying dATP-induced changes in heart metabolism. To achieve this, we conducted *in vitro* assays of CK8m-RNR$_{DM}$-CMs to study the CM-specific effects of chronic dATP elevation. Targeted metabolomics of the CK8m-RNR$_{DM}$-CMs showed greater TCA intermediates such as aconitate, succinate, and α-ketoglutarate as compared to WT-CMs (Fig. 5E), together with slightly increased ATP that would likely improve cellular energetics. CK8m-RNR$_{DM}$-CMs also had elevated levels of acyl-carnitines, free fatty acids, and intermediate products of oxidative decomposition of fatty acids compared to WT-CMs, suggesting increased fatty acid metabolism. Overall, CK8m-RNR$_{DM}$-CMs had greater levels of metabolites in oxidative phosphorylation and energy generation (Fig. 5E).

We performed bioenergetic flux analysis to study metabolic differences in the living cells used for transplants. The CK8m-RNR$_{DM}$-CMs exhibited elevated basal respiration (89.1±8.9 vs. 61.3±7.4 pmoles O_2/min/μg protein) (Fig. 5F, G), maximal respiration (175.4±21.5 vs. 86.9±11.3 pmoles O_2/min/μg protein), and spare respiratory capacity (86.2±16.7 vs. 25.6±5.2 pmoles O_2/min/μg protein) compared to WT-CMs (Fig. 5G). To further dissect the underlying mechanisms, we determined mitochondrial DNA (mtDNA, UUR gene) content normalized to nuclear DNA content (nuDNA, B2M gene) (Fig. 5H). The CK8m-RNR$_{DM}$-CMs had 2.1-fold greater mtDNA than WT-CMs ($p \leq 0.05$), indicating a substantial induction of mitochondrial biogenesis. Taken together, these bioenergetic studies demonstrate that CK8m-RNR$_{DM}$-CMs have greater oxidative metabolic capacity than WT-CMs.

WITHDRAWN see manuscript DOI for details

bioRxiv preprint doi: https://doi.org/10.1101/2023.04.24.538108; this version posted April 28, 2023. The copyright holder for this preprint (which was not certified by peer review) is the author/funder, who has granted bioRxiv a license to display the preprint in perpetuity. It is made available under a CC-BY-ND 4.0 International license.



WITHDRAWN
see manuscript DOI for details

Fig. 5 CK8m-RNR$_{DM}$-CMs therapy induces a dynamic metabolic shift in chronic MI. Relative difference in selected metabolites detected by targeted metabolomics in hearts at the endpoint of the Chronic MI study related to **(A)** TCA cycle, **(B)** Glycolysis **(C)** Fatty acid oxidation **(D)** Energetics. N=4 animals per group. Each symbol represents biological replicate where open circles (No-cells), solid circle (WT-CMs), solid triangles (CK8m-RNR$_{DM}$-CMs)). **(E)** Heat-map depicting relative

bioRxiv preprint doi: https://doi.org/10.1101/2023.04.24.538108; this version posted April 28, 2023. The copyright holder for this preprint (which was not certified by peer review) is the author/funder, who has granted bioRxiv a license to display the preprint in perpetuity. It is made available under a CC-BY-ND 4.0 International license.

abundance of selected metabolites in CK8m-RNR$_{DM}$-CMs vs. WT-CMs, N=4 independent differentiations/cell line **(F)** Oxygen consumption rate (OCR) trace in CK8m-RNR$_{DM}$-CMs vs. WT-CMs. **(G)** Bar graphs depicting basal, maximal, and spare respiratory capacity. Each symbol represents technical replicate where solid circle (WT-CMs) and solid triangles (CK8m-RNR$_{DM}$-CMs)). N=3 independent differentiations/cell line, n=3 technical replicates /differentiation. **(H)** Mitochondrial (mtDNA): nuclear DNA (nuDNA) ratios in CK8m-RNR$_{DM}$-CMs vs. WT-CMs, normalized to WT ratio, N=4 independent differentiations/cell line. P values (metabolites) were determined using Kruskal Wallis with Dunn's correction or one- way ANOVA with Sidak's multiple comparisons, *P<0.05, **P<0.01. P values (cellular energetics and mitochondrial content) were determined by Student t test, *P<0.05, **P<0.01. All data are presented as mean ± S.E.M. (Panel A and E were created with Biorender.com).

Discussion

WITHDRAWN
see manuscript DOI for details

The application of hPSC-CM-based cell therapy for Chronic MI has been challenging, mainly due to the profound dysfunction of residual host cardiomyocytes, the inability to resorb or remodel matured scar, inefficient energetics, and insufficient remuscularization. Our goal was to improve regenerative strategies by genome-editing hPSC to make dATP-donor cells that can perform dual functions of replacing damaged myocardium while delivering dATP to the native myocardium to boost contractility in dysfunctional host cardiomyocytes (*20*)(*18*). Our results indicate that dATP donor CMs (CK8m-RNR$_{DM}$-CMs) can remuscularize and persistently improve the function of the chronically injured heart in ways that enhance exercise behavior and reduce mortality.

Our initial concern that activating myosin throughout the failing heart might worsen the heart's energy imbalance proved unfounded. Instead, donor cells shifted their recipient heart's metabolism from glycolysis to oxidative phosphorylation and improved energy balance, whereas the No-cells and WT-CMs recipients exhibited a more glycolytic profile, characteristic of HF. Earlier, our biochemical and molecular modeling studies (*30*)(*31*) have shown that dATP induces structural and mechanical changes in cardiac muscle myosin which can improve CM energetics (*32*). Moreover, sustained elevated cellular and mitochondrial dATP have beneficial effects such as remodeling of cellular metabolic pathways and mitochondria in the heart (*19*). Thus, the dATP donor cells are uniquely robust toward improving cardiac function as well as physiological function at the organismal level.

Interventions to increase the contractility of the failing heart have been sought for decades. This has challenged drug developers due to the increased lethal arrhythmias associated with agents that elevate intracellular Ca^{2+} levels in cardiomyocytes (*33*). Our novel strategy of cell therapy-mediated, cardiac-specific elevation of dATP targets cardiac myosin directly without increasing Ca^{2+} levels (*34*), bypassing this arrhythmogenic trigger. In support of this idea, the small molecule myosin activator, Omecamtiv mecarbil, recently was shown to reduce hospitalizations in patients with chronic heart failure while having no adverse effect on mortality (*35*). The allosteric activation of cardiac myosins by dATP is widely conserved across species (*17*, *18*, *34*). Importantly, we previously showed that dATP augments contractility in permeabilized myocardial strips from failing human hearts (*36*), supporting the hypothesis that dATP donor cells would improve function in patients with HF. While substantial recent progress has been made in reducing the arrhythmias associated with hPSC-CM therapy (*37*, *38*), remaining challenges to hPSC-CM therapy include immunogenicity of allogeneic cells, scaled manufacturing, delivery to the heart, and absence of tumor formation in a longer-term follow-up. Further studies may provide information on the optimization of dose, delivery, efficacy, and safety.

bioRxiv preprint doi: https://doi.org/10.1101/2023.04.24.538108; this version posted April 28, 2023. The copyright holder for this preprint (which was not certified by peer review) is the author/funder, who has granted bioRxiv a license to display the preprint in perpetuity. It is made available under a CC-BY-ND 4.0 International license.

Overall, therapeutic applications of these dATP donor cell lines can be envisioned beyond ischemic heart disease, e.g., dilated cardiomyopathy, thereby benefiting the greater chronic HF population with reduced function.

References and Notes:

1. C. W. Tsao, A. W. Aday, Z. I. Almarzooq, C. A. M. Anderson, P. Arora, C. L. Avery, C. M. Baker-Smith, A. Z. Beaton, A. K. Boehme, A. E. Buxton, Y. Commodore-Mensah, M. S. V. Elkind, K. R. Evenson, C. Eze-Nliam, S. Fugar, G. Generoso, D. G. Heard, S. Hiremath, J. E. Ho, R. Kalani, D. S. Kazi, D. Ko, D. A. Levine, J. Liu, J. Ma, J. W. Magnani, E. D. Michos, M. E. Mussolino, S. D. Navaneethan, N. I. Parikh, R. Poudel, M. Rezk-Hanna, G. A. Roth, N. S. Shah, M.-P. St-Onge, E. L. Thacker, S. S. Virani, J. H. Voeks, N.-Y. Wang, N. D. Wong, S. S. Wong, K. Yaffe, S. S. Martin, Heart Disease and Stroke Statistics-2023 Update: A Report From the American Heart Association. *Circulation* (2023), doi:10.1161/CIR.0000000000001123.
2. A. Bertero, C. E. Murry, Hallmarks of cardiac regeneration. *Nat. Rev. Cardiol.* **15** (2018), pp. 579–580.
3. L. K. Truby, J. G. Rogers, Advanced Heart Failure: Epidemiology, Diagnosis, and Therapeutic Approaches. *JACC Hear. Fail.* **8** (2020), pp. 523–536.
4. M. Yacoub, Cardiac donation after circulatory death: A time to reflect. *Lancet*. **385** (2015), pp. 2554–2556.
5. A Study of iPS Cell-derived Cardiomyocyte Spheroids (HS-001) in Patients With Heart Failure (LAPiS Study) (LAPiS) (2021), (available at https://www.clinicaltrials.gov/ct2/show/NCT04945018).
6. Nct, Treating Congestive HF With hiPSC-CMs Through Endocardial Injection. *https://clinicaltrials.gov/show/NCT04982081* (2021) (available at https://www.clinicaltrials.gov/ct2/show/NCT04982081).
7. H. Zhang, Y. Xue, T. Pan, X. Zhu, H. Chong, C. Xu, F. Fan, H. Cao, B. Zhang, J. Pan, Q. Zhou, G. Yang, J. Wang, D. J. Wang, Epicardial injection of allogeneic human-induced-pluripotent stem cell-derived cardiomyocytes in patients with advanced heart failure: Protocol for a phase I/IIa dose-escalation clinical trial. *BMJ Open*. **12** (2022), doi:10.1136/bmjopen-2021-056264.
8. Safety and Efficacy of Induced Pluripotent Stem Cell-derived Engineered Human Myocardium as Biological Ventricular Assist Tissue in Terminal Heart Failure - Full Text View - ClinicalTrials.gov, (available at https://www.clinicaltrials.gov/ct2/show/NCT04396899).
9. Y. Shiba, S. Fernandes, W. Z. Zhu, D. Filice, V. Muskheli, J. Kim, N. J. Palpant, J. Gantz, K. W. Moyes, H. Reinecke, B. Van Biber, T. Dardas, J. L. Mignone, A. Izawa, R. Hanna, M. Viswanathan, J. D. Gold, M. I. Kotlikoff, N. Sarvazyan, M. W. Kay, C. E. Murry, M. A. Laflamme, Human ES-cell-derived cardiomyocytes electrically couple and suppress arrhythmias in injured hearts. *Nature*. **489**, 321–326 (2012).
10. K. A. Gerbin, X. Yang, C. E. Murry, K. L. K. Coulombe, Enhanced electrical integration of engineered human myocardium via intramyocardial versus epicardial delivery in infarcted rat hearts. *PLoS One*. **10**, 1–13 (2015).
11. T. Stüdemann, J. Rössinger, C. Manthey, B. Geertz, R. Srikantharajah, C. Von Bibra, A. Shibamiya, M. Köhne, A. Wiehler, J. S. Wiegert, T. Eschenhagen, F. Weinberger, Contractile Force of Transplanted Cardiomyocytes Actively Supports Heart Function after Injury. *Circulation*. **146**, 1159–1169 (2022).
12. Y. W. Liu, B. Chen, X. Yang, J. A. Fugate, F. A. Kalucki, A. Futakuchi-Tsuchida, L. Couture, K. W. Vogel, C. A. Astley, A. Baldessari, J. Ogle, C. W. Don, Z. L. Steinberg, S. P. Seslar, S. A. Tuck, H. Tsuchida, A. V Naumova, S. K. Dupras, M. S. Lyu, J. Lee, D. W. Hailey, H. Reinecke, L. Pabon, B. H. Fryer, W. R. MacLellan, R. S. Thies, C. E. Murry, Human embryonic stem cell-

WITHDRAWN
See manuscript DOI for details

bioRxiv preprint doi: https://doi.org/10.1101/2023.04.24.538108; this version posted April 28, 2023. The copyright holder for this preprint (which was not certified by peer review) is the author/funder, who has granted bioRxiv a license to display the preprint in perpetuity. It is made available under a CC-BY-ND 4.0 International license.

derived cardiomyocytes restore function in infarcted hearts of non-human primates. *Nat. Biotechnol.* **36**, 597–605 (2018).

13. Y. Shiba, D. Filice, S. Fernandes, E. Minami, S. K. Dupras, B. Van Biber, P. Trinh, Y. Hirota, J. D. Gold, M. Viswanathan, M. A. Laflamme, Electrical integration of human embryonic stem cell-derived cardiomyocytes in a guinea pig chronic infarct model. *J. Cardiovasc. Pharmacol. Ther.* **19**, 368–381 (2014).
14. S. Fernandes, A. V. Naumova, W. Z. Zhu, M. A. Laflamme, J. Gold, C. E. Murry, Human embryonic stem cell-derived cardiomyocytes engraft but do not alter cardiac remodeling after chronic infarction in rats. *J. Mol. Cell. Cardiol.* **49**, 941–949 (2010).
15. K. S. Thomson, G. L. Odom, C. E. Murry, G. G. Mahairas, Translation of Cardiac Myosin Activation. *J. Am. Coll. Cardiol.* **1**, 666–679 (2016).
16. S. G. Nowakowski, S. C. Kolwicz, F. S. Korte, Z. Luo, J. N. Robinson-Hamm, J. L. Page, F. Brozovich, R. S. Weiss, R. Tian, C. E. Murry, M. Regnier, Transgenic overexpression of ribonucleotide reductase improves cardiac performance. *Proc. Natl. Acad. Sci.* **110**, 6187–6192 (2013).
17. S. C. Kolwicz, G. L. Odom, S. G. Nowakowski, F. Moussavi-Harami, X. Chen, H. Reinecke, S. D. Hauschka, C. E. Murry, G. G. Mahairas, M. Regnier, AAV6-mediated cardiac-specific overexpression of ribonucleotide reductase enhances myocardial contractility. *Mol. Ther.* **24**, 240–250 (2016).
18. S. Kadota, J. Carey, H. Reinecke, J. Leggett, S. Teichman, M. A. Laflamme, C. E. Murry, M. Regnier, G. G. Mahairas, Ribonucleotide reductase-mediated increase in dATP improves cardiac performance via myosin activation in a large animal model of heart failure. *Eur. J. Heart Fail.* **17**, 772–781 (2015).
19. K. N. Mhatre, J. D. Murray, G. Flint, T. S. McMillen, G. Weber, M. Shakeri, A. Y. Tu, S. Steczina, R. Weiss, D. J. Marcinek, C. E. Murry, D. Raftery, R. Tian, F. Moussavi-Harami, M. Regnier, dATP elevation induces myocardial metabolic remodeling to support improved cardiac function. *J. Mol. Cell. Cardiol.* **175**, 1–12 (2023).
20. S. D. Lundy, S. A. Murphy, S. K. Dupras, J. Dai, C. E. Murry, M. A. Laflamme, M. Regnier, Cell-based delivery of dATP via gap junctions enhances cardiac contractility. *J. Mol. Cell. Cardiol.* **72**, 350–359 (2014).
21. W. Qiu, B. Zhou, D. Darwish, J. Shao, Y. Yen, Characterization of enzymatic properties of human ribonucleotide reductase holoenzyme reconstituted in vitro from hRRM1, hRRM2, and p53R2 subunits. *Biochem. Biophys. Res. Commun.* **340**, 428–434 (2006).
22. V. D'Angiolella, V. Donato, F. M. Forrester, Y. T. Jeong, C. Pellacani, Y. Kudo, A. Saraf, L. Florens, M. P. Washburn, M. Pagano, Cyclin F-mediated degradation of ribonucleotide reductase M2 controls genome integrity and DNA repair. *Cell*. **149**, 1023–1034 (2012).
23. A. L. Chabes, C. M. Pfleger, M. W. Kirschner, L. Thelander, Mouse ribonucleotide reductase R2 protein: A new target for anaphase-promoting complex-Cdh1-mediated proteolysis. *Proc. Natl. Acad. Sci. U. S. A.* **100**, 3925–3929 (2003).
24. S. Olafsson, D. Whittington, J. Murray, M. Regnier, F. Moussavi-Harami, Fast and sensitive HPLC–MS/MS method for direct quantification of intracellular deoxyribonucleoside triphosphates from tissue and cells. *J. Chromatogr. B Anal. Technol. Biomed. Life Sci.* **1068–1069**, 90–97 (2017).
25. M. A. Laflamme, K. Y. Chen, A. V Naumova, V. Muskheli, J. A. Fugate, S. K. Dupras, H. Reinecke, C. Xu, M. Hassanipour, S. Police, C. O'Sullivan, L. Collins, Y. Chen, E. Minami, E. A. Gill, S. Ueno, C. Yuan, J. Gold, C. E. Murry, Cardiomyocytes derived from human embryonic stem cells in pro-survival factors enhance function of infarcted rat hearts. *Nat. Biotechnol.* **25**, 1015–1024 (2007).

WITHDRAWN
see manuscript DOI for details

bioRxiv preprint doi: https://doi.org/10.1101/2023.04.24.538108; this version posted April 28, 2023. The copyright holder for this preprint (which was not certified by peer review) is the author/funder, who has granted bioRxiv a license to display the preprint in perpetuity. It is made available under a CC-BY-ND 4.0 International license.

26. J. McCoy, M. Bates, C. Eggett, M. Siervo, S. Cassidy, J. Newman, S. A. Moore, G. Gorman, M. I. Trenell, L. Velicki, P. M. Seferovic, J. G. F. Cleland, G. A. MacGowan, D. M. Turnbull, D. G. Jakovljevic, Pathophysiology of exercise intolerance in chronic diseases: The role of diminished cardiac performance in mitochondrial and heart failure patients. *Open Hear.* **4** (2017), doi:10.1136/openhrt-2017-000632.

27. G. M. Long, A. D. Troutman, D. A. Gray, A. J. Fisher, T. Lahm, A. R. Coggan, M. B. Brown, Skeletal muscle blood flow during exercise is reduced in a rat model of pulmonary hypertension. *Am. J. Physiol. - Regul. Integr. Comp. Physiol.* **323**, R561–R570 (2022).

28. M. Sugihara, F. Odagiri, T. Suzuki, T. Murayama, Y. Nakazato, K. Unuma, K. I. Yoshida, H. Daida, T. Sakurai, S. Morimoto, N. Kurebayashi, Usefulness of Running Wheel for Detection of Congestive Heart Failure in Dilated Cardiomyopathy Mouse Model. *PLoS One*. **8** (2013), doi:10.1371/JOURNAL.PONE.0055514.

29. G. D. Lopaschuk, Q. G. Karwi, R. Tian, A. R. Wende, E. D. Abel, Cardiac Energy Metabolism in Heart Failure. *Circ. Res.* **128**, 1487–1513 (2021).

30. J. D. Powers, C. C. Yuan, K. J. McCabe, J. D. Murray, M. C. Childers, G. V. Flint, F. Moussavi-Harami, S. Mohran, R. Castillo, C. Zuzek, W. Ma, V. Daggett, A. D. McCulloch, T. C. Irving, M. Regnier, Cardiac myosin activation with 2-deoxy-ATP via increased electrostatic interactions with actin. *Proc. Natl. Acad. Sci. U. S. A.* **166**, 11502–11507 (2019).

31. J. Walklate, K. Kao, M. Regnier, M. A. Geeves, Exploring the super-relaxed state of myosin in myofibrils from fast-twitch, slow-twitch, and cardiac muscle. *J. Biol. Chem.* **298** (2022), p. 101640.

32. C. N. Toepfer, A. C. Garfinkel, G. Venturini, H. Wakimoto, G. Repetti, L. Alamo, A. Sharma, R. Agarwal, J. F. Ewoldt, P. Cloonan, J. Letendre, M. Lun, I. Olivotto, S. Colan, E. Ashley, D. Jacoby, M. Michels, C. S. Redwood, H. C. Watkins, S. M. Day, J. F. Staples, R. Padrón, A. Chopra, C. Y. Ho, C. S. Chen, A. C. Pereira, J. G. Seidman, C. E. Seidman, Myosin Sequestration Regulates Sarcomere Function, Cardiomyocyte Energetics, and Metabolism, Informing the Pathogenesis of Hypertrophic Cardiomyopathy. *Circulation*, 828–842 (2020).

33. C. Maack, T. Eschenhagen, N. Hamdani, F. R. Heinze, A. R. Lyon, D. J. Manstein, J. Metzger, Z. Papp, C. G. Tocchetti, M. B. Yilmaz, S. D. Anker, J. L. Balligand, J. Bauersachs, D. Brutsaert, L. Carrier, S. Chlopicki, J. G. Cleland, R. A. De Boer, A. Dietl, R. Fischmeister, V. P. Harjola, S. Heymans, D. Hilfiker-Kleiner, J. Holzmeister, G. De Keulenaer, G. Limongelli, W. A. Linke, L. H. Lund, J. Masip, M. Metra, C. Mueller, B. Pieske, P. Ponikowski, A. Risti, F. Ruschitzka, P. M. Seferovi, H. Skouri, W. H. Zimmermann, A. Mebazaa, Treatments targeting inotropy. *Eur. Heart J.* **40**, 3626-3640D (2019).

34. F. S. Korte, J. Dai, K. Buckley, E. R. Feest, N. Adamek, M. A. Geeves, C. E. Murry, M. Regnier, Upregulation of cardiomyocyte ribonucleotide reductase increases intracellular 2 deoxy-ATP, contractility, and relaxation. *J. Mol. Cell. Cardiol.* **51**, 894–901 (2011).

35. J. R. Teerlink, R. Diaz, G. M. Felker, J. J. V. McMurray, M. Metra, S. D. Solomon, K. F. Adams, I. Anand, A. Arias-Mendoza, T. Biering-Sørensen, M. Böhm, D. Bonderman, J. G. F. Cleland, R. Corbalan, M. G. Crespo-Leiro, U. Dahlström, L. E. Echeverria, J. C. Fang, G. Filippatos, C. Fonseca, E. Goncalvesova, A. R. Goudev, J. G. Howlett, D. E. Lanfear, J. Li, M. Lund, P. Macdonald, V. Mareev, S. Momomura, E. O'Meara, A. Parkhomenko, P. Ponikowski, F. J. A. Ramires, P. Serpytis, K. Sliwa, J. Spinar, T. M. Suter, J. Tomcsanyi, H. Vandekerckhove, D. Vinereanu, A. A. Voors, M. B. Yilmaz, F. Zannad, L. Sharpsten, J. C. Legg, C. Varin, N. Honarpour, S. A. Abbasi, F. I. Malik, C. E. Kurtz, Cardiac Myosin Activation with Omecamtiv Mecarbil in Systolic Heart Failure. *N. Engl. J. Med.* **384**, 105–116 (2021).

36. F. Moussavi-Harami, M. V. Razumova, A. W. Racca, Y. Cheng, A. Stempien-Otero, M. Regnier, 2-Deoxy adenosine triphosphate improves contraction in human end-stage heart failure.

WITHDRAWN
see manuscript DOI for details

bioRxiv preprint doi: https://doi.org/10.1101/2023.04.24.538108; this version posted April 28, 2023. The copyright holder for this preprint (which was not certified by peer review) is the author/funder, who has granted bioRxiv a license to display the preprint in perpetuity. It is made available under a CC-BY-ND 4.0 International license.

J. Mol. Cell. Cardiol. **79**, 256–263 (2015).

37. K. Nakamura, L. E. Neidig, X. Yang, G. J. Weber, D. El-Nachef, H. Tsuchida, S. Dupras, F. A. Kalucki, A. Jayabalu, A. Futakuchi-Tsuchida, D. S. Nakamura, S. Marchianò, A. Bertero, M. R. Robinson, K. Cain, D. Whittington, R. Tian, H. Reinecke, L. Pabon, B. C. Knollmann, S. Kattman, R. S. Thies, W. R. MacLellan, C. E. Murry, Pharmacologic therapy for engraftment arrhythmia induced by transplantation of human cardiomyocytes. *Stem Cell Reports*. **16**, 2473–2487 (2021).
38. S. Marchiano, K. Nakamura, H. Reinecke, L. Neidig, M. Lai, S. Kadota, F. Perbellini, X. Yang, J. M. Klaiman, L. Blakley, E. Karbassi, P. Feilds, A. M. Fenix, K. M. Beussman, A. Jayabalu, F. A. Kalucki, A. Futakuchi-Tsuchida, G. J. Weber, S. K. Dupras, H. Tsuchida, L. Pabon, L. Wang, B. C. Knollmann, S. Kattman, S. Theis, N. J. Sniadecki, W. Robb MacLellan, A. Bertero, W. R. Maclellan, A. Bertero, C. E. Murry, Gene editing to prevent ventricular arrhythmias associated with cardiomyocyte cell therapy. *Cell Stem Cell*. **30**, 1–19 (2023).
39. J. N. Ramos, K. Hollinger, N. E. Bengtsson, J. M. Allen, S. D. Hauschka, J. S. Chamberlain, Development of Novel Micro-dystrophins with Enhanced Functionality. *Mol. Ther.* **27**, 623–635 (2019).
40. F. Oceguera-Yanez, S. Il Kim, T. Matsumoto, G. W. Tan, L. Xiang, T. Hatani, T. Kondo, M. Ikeya, Y. Yoshida, H. Inoue, K. Woltjen, Engineering the AAVS1 locus for consistent and scalable transgene expression in human iPSCs and their differentiated derivatives. *Methods*. **101**, 43–55 (2016).
41. K. A. Gerbin, K. A. Mitzelfelt, X. Guan, A. M. Martinson, C. E. Murry, Delta-1 Functionalized Hydrogel Promotes hESC-Cardiomyocyte Graft Proliferation and Maintains Heart Function Post-Injury. *Mol. Ther. - Methods Clin. Dev.* **17**, 986–998 (2020).
42. P. W. Burridge, E. Matsa, P. Shukla, Z. C. Lin, J. M. Churko, A. D. Ebert, F. Lan, S. Diecke, B. Huber, N. M. Mordwinkin, J. R. Plews, O. J. Abilez, B. Cui, J. D. Gold, J. C. Wu, Chemically defined generation of human cardiomyocytes. *Nat. Methods*. **11**, 855–860 (2014).

Acknowledgments: We thank the University of Washington (UW) Department of Comparative Medicine for their exceptional veterinary care and consultation for the animal experiments. We also thanks Dylan Brunette and Cathy Sanford for their help and experimental support. This research was assisted by the UW Cell Analysis Facility (Department of Immunology), the Lynn and Mike Garvey Cell Imaging Core (Institute for Stem Cell and Regenerative Medicine), Tom & Sue Ellison Stem Cell Core (Institute for Stem Cell and Regenerative Medicine), The CRISPR, Vector and Transgenic Mouse Core (UW Diabetes Research Center), and Specialty VETPATH for histology services. The AAV6 vector production was carried out by the Sen. Paul D. Wellstone Muscular Dystrophy Specialized Research Center-Vector Core, UW.

Funding: These studies were supported in part by
National Institutes of Health grant R01 HL128368 (to M.R. and C.E.M.),
National Institutes of Health grant R01 HL146868 (to C.E.M.),
National Institutes of Health grant R01 HL160825 (to C.E.M.) and
National Institutes of Health grant K08 HL128826 (to F.M.H.).
Some resources were provided by the UW Center for Translational Muscle Research which is funded by
National Institutes of Health grant P30 AR074990 (to M.R., D.R), and
National Institutes of Health grant S10 OD021562 (to D.R).
The research leading to CK8m promoter was supported by a
Wellstone Center Grant PO-50-AR-065139 (to S.D.H.).

WITHDRAWN
see manuscript DOI for details

bioRxiv preprint doi: https://doi.org/10.1101/2023.04.24.538108; this version posted April 28, 2023. The copyright holder for this preprint (which was not certified by peer review) is the author/funder, who has granted bioRxiv a license to display the preprint in perpetuity. It is made available under a CC-BY-ND 4.0 International license.

State of Washington UW Institute for Stem Cells and Regenerative Medicine fellows' program (to K.M.)
National Institutes of Health grant S10OD024979 (UW Cell Analysis Facility).

Author contributions:

KNM, CEM, MR conceived the project and designed experiments.
KNM, JM, AT, HR, XY, XG, EM, GLO, SDH, DR, RT, FMH performed experiments and interpreted *in vitro* experiments.
KNM, AM, GF, LPB, JMK, MBB performed experiments and interpreted *in vivo* experiments.
KNM wrote the manuscript.
CEM, MR, JMK, FMH, SDH, GLO, MBB reviewed and edited the manuscript.

Competing interests: M.R., C.E.M., K.N.M., and S.D.H. are inventors (University of Washington) on a patent for (US Utility Patent application # PCT/US2023/062377 filed on 10th February 2023). Some of these studies were performed while C.E.M. was an employee of Sana Biotechnology; C.E.M. is also an equity holder in Sana Biotechnology. S.D.H. has a pending patent regarding CK8m promoter. Authors declare that they have no competing interests.

Data and materials availability: We have signed MTA agreement for usage of CK8m promoter with S.D.H. (University of Washington). All data are available in the main text or the supplementary materials.

WITHDRAWN
see manuscript DOI for details